Chapter 3
Role of Optical Coherence Tomography in Glaucoma

Ahmet Akman

3.1 Introduction

Retinal ganglion cells (RGC) are large, complex neurons, which are the main cells affected in glaucoma. Dendrites of the RGCs make synapses with bipolar and amacrine cells in the inner plexiform layer (IPL) of the retina. Cell bodies of the RGCs make up the ganglion cell layer (GCL) and their axons form the retinal nerve fiber layer (RNFL). All the axons in the RNFL converge at the optic nerve head (ONH) to form the neuro-retinal rim. The RGC axons synapse in the lateral geniculate body with the third neuron of the visual pathway.

Optical Coherence Tomography (OCT) has revolutionized the diagnosis and monitoring of glaucoma as it can detect RGC damage objectively and quantitatively [1]. As structural damage frequently precedes functional damage, methods that are able to identify structural damage are of utmost importance for early diagnosis of glaucoma [2–4]. For decades, the only tool available for diagnosing glaucoma with structural means was clinical observation of the changes on ONH photographs. With the advent of digital imaging methods such as scanning laser polarimetry and confocal scanning laser systems, objective and quantitative evaluation of the ONH and RNFL became possible [5–7]. OCT has replaced these systems over the last decade and has become the gold standard for detecting early structural glaucomatous damage, as it can evaluate RNFL, macular ganglion cell and ONH changes at the same time with high reproducibility and reliability [7–11]. Kuang et al. demonstrated that OCT could detect glaucomatous damage 5 years prior to appearance of the first visual field (VF) defects in one third of patients based on average RNFL thickness measurements [12].

The 10th World Glaucoma Association Consensus publication, published in 2016, stated that, detecting progressive glaucomatous RNFL thinning and neuroretinal

A. Akman
Department of Ophthalmology, School of Medicine, Başkent University, Ankara, Turkey

A. Akman et al. (eds.), *Optical Coherence Tomography in Glaucoma*,
https://doi.org/10.1007/978-3-319-94905-5_3

rim narrowing are the best available gold standards for glaucoma diagnosis. Detection of VF defects is not imperative for the diagnosis of glaucoma and OCT is the best currently available digital imaging technology for detecting structural damage in glaucoma [13].

Figure 3.1 summarizes the timeline of changes in glaucomatous eyes demonstrating disease progression. In the preperimetric stages of the disease, RNFL loss is the first sign of structural damage followed by or accompanied by ONH changes. Animal data have shown that neuroretinal changes may precede RNFL loss although clinical evidence is still lacking [14]. As the disease progresses to the perimetric stage, VF changes start to emerge. The relationship of these structural and functional tests in glaucoma will be discussed in detail in Chap. 16.

Among the three parameters that can be evaluated with OCT, RNFL thickness measurements are the most widely studied. RNFL thickness parameters were the main outcome to be measured in the TD-OCT era. With the higher resolution and denser sampling capabilities of SD-OCT, reliable Ganglion Cell Analysis became a possibility. Finally, SD-OCT allowed imaging of the ONH anatomic features with great precision and led to development of newer outcome measures such as the Bruch's membrane opening (BMO) based minimum rim width (MRW). The aim of this chapter is to summarize the role of these three approaches in clinical practice for the diagnosis of glaucoma.

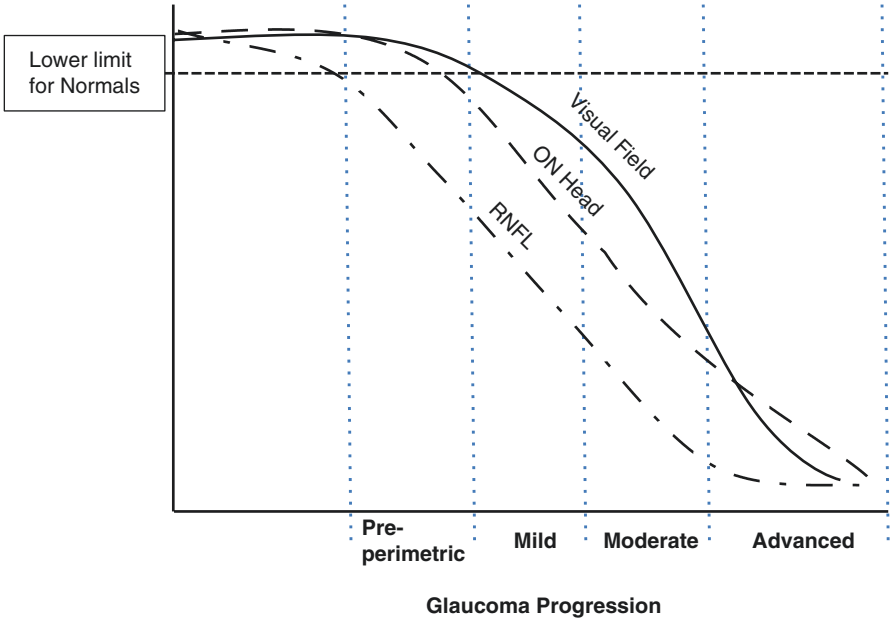

Fig. 3.1 Timeline of structural and functional changes in glaucoma. (Modified form original slide by Weinreb RN, Robert N. Shaffer Lecture at the 105th Annual Meeting of the American Academy of Ophthalmology, New Orleans, 2001, with permission from Robert N. Weinreb)

3.2 RNFL Analysis

Quigley and associates showed that RNFL changes frequently preceded ONH changes [10]. However, RNFL thinning is difficult to identify on routine fundus examination. To overcome this obstacle, various imaging modalities have been used in the past to detect peripapillary RNFL loss, including red free photography, scanning laser polarimetry and confocal scanning laser ophthalmoscopy. Since the availability of OCT, it has become the preferred technique for RNFL analysis in eyes with suspected or established glaucoma [15].

There are two basic strategies for peripapillary RNFL analysis with OCT. The first one is to scan and construct a three-dimensional map of the RNFL around the ONH. Current Carl Zeiss Meditec (Dublin, CA), Topcon Medical Systems (Oakland, NJ) and Optovue Inc. (Fremont, CA) SD-OCT systems construct these maps, which provide a detailed analysis of RNFL changes included in the cube. The second and most studied strategy is to measure the peripapillary RNFL thickness on a 3.46 mm scan circle centered on the ONH or BMO. This circle is called the calculation circle in Zeiss Cirrus HD-OCT as it is calculated from the 6 × 6mm Optic Disc Cube. On the other hand, Heidelberg Spectralis OCT (Heidelberg Engineering, Heidelberg, Germany) does not use a scan cube for RNFL measurements. It uses data from a single 3.46 mm circular scan around the ONH and names this circle the scan circle. The newer software on the Heidelberg Spectralis OCT (Glaucoma Module Premium Edition, GMPE) now measures the RNFL on 3 concentric circles centered on the BMO at 3.46, 4.1, and 4.7 mm diameters. Also, other instruments and some other authors use the term ‘measurement circle’ for this. As the calculation circle, measurement circle and scan circle are terms that define the same 3.46 mm circle, they are used interchangeably depending on the OCT device throughout this book.

3.2.1 RNFL Thickness Map

SD-OCT devices can scan the ONH area in a few seconds and construct three-dimensional maps of the RNFL around the ONH with high precision. Figure 3.2 shows RNFL thickness map scans from different OCT devices. Different OCT devices use different scan cube sizes; Cirrus HD-OCT scans a 6 × 6 mm area comprised of 200 horizontal scans each consisting of 200 A-scans resulting in a three-dimensional RNFL thickness map with a resolution of 200 × 200 A-scans. Each A-scan corresponds to a 30-micron square of the retina in an emmetropic eye. RNFL changes across the 6 × 6 mm (200 × 200 pixel) area around the ONH may detect RNFL loss better compared to a single 3.46 mm circumpapillary RNFL scan [16–18].

Leung et al. compared the RNFL thickness map with the circumpapillary RNFL calculation circle data and concluded that the former significantly improved diagnostic sensitivity by providing additional spatial and morphologic information

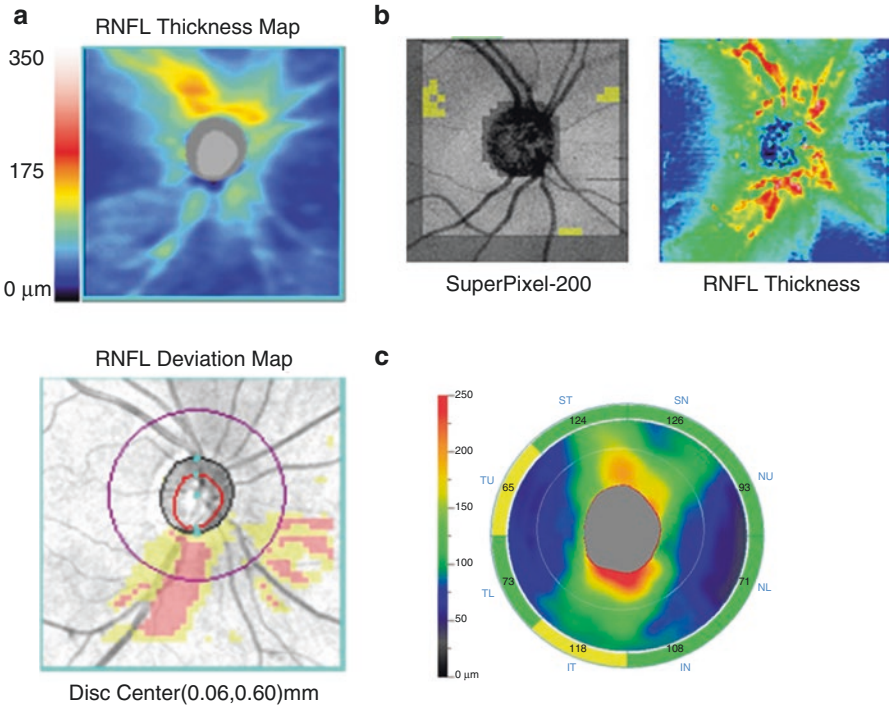

Fig. 3.2 RNFL thickness maps from three SD-OCT devices. (**a**). Zeiss Cirrus HD-OCT (pseudo-color RNFL thickness map, RNFL deviation map), (**b**) Topcon 3D OCT 2000 (RNFL deviation map, pseudo-color thickness map), and (**c**) Optovue (pseudo-color thickness map)

about RNFL damage [18]. In another study, the same group showed that the most common location for RNFL thinning was at the infero-temporal meridians approximately 2 mm from the disc center. As the radius of the 3.46 mm calculation circle is 1.73 mm, RNFL thickness map scan is required to show changes in this region, which is outside the confines of the 3.46 mm calculation circle [17].

3.2.2 The RNFL Calculation Circle

Peripapillary RNFL measurement based on the calculation circle is the most frequently used method for evaluating RNFL loss. In the early days of OCT, TD-OCT systems did not have enough resolution and scan speed to construct RNFL thickness maps; hence, only a single circumpapillary RNFL scan centered on the ONH was utilized. The scan circle was set to an arbitrary 3.4 mm diameter based on an earlier study by Schuman et al. [19]. Subsequently, all OCT manufacturers adopted the 3.46 mm scan circle and it became the standard for glaucoma diagnostic studies in the literature. Apart from this 3.46 mm scan circle, which is available in all current

OCT devices, the GMPE software of Spectralis OCT has 4.1 and 4.7 mm scan circle options although their clinical significance is yet to be determined. Current SD-OCT devices center the 3.46 mm scan circle on the ONH Bruch's membrane opening (BMO) centroid automatically. The role of BMO in glaucoma diagnostics will be discussed in detail under ONH analysis in Sect. 3.4.

3.2.2.1 The RNFL Calculation Circle and TSNIT Plots

Circumpapillary RNFL calculation or circular scan data can be presented in many different formats. Each manufacturer has their own preferred format for this purpose. Most OCT devices provide average, hemifield, quadrant and clock hour sector thickness measurements. In addition, the numeric data are often presented on false color (pseudo-color) maps or with pie graphs.

One common plot used by all OCT platforms is the TSNIT plot for reporting the RNFL thickness values along the calculation or scan circle. TSNIT maps were originally used to display RNFL thickness measurements on GDx device (Laser Diagnostic Technologies, San Diego, CA), which measures RNFL thicknesses based on scanning laser polarimetry. With the evolution of OCT, scanning laser polarimetry lost its popularity but many of the presentation concepts for RNFL measurements and analysis were adopted for OCT reports.

The segmentation algorithm of the OCT software identifies the RNFL and measures the RNFL thickness on the circular peripapillary scan. The RNFL measurements along the calculation or scan circle are then plotted starting from temporal quadrant (9 o'clock in the right eye, 3 o'clock in the left eye) in a clockwise fashion for the right eye and counterclockwise fashion for the left eye as TSNIT plot. TSNIT stands for **T**emporal **S**uperior **N**asal **I**nferior **T**emporal locations (Fig. 3.3). The RNFL thickness values are displayed along the calculation circle starting temporally, moving superiorly, nasally, inferiorly and ending temporally. The direction is clockwise for the right eye and counterclockwise for the left eye. Normally, a double hump pattern is visible on the TSNIT plot with the peak RNFL areas located in the superior and inferior quadrants. Comparisons to the normative database of any given OCT device is performed and the probability values for abnormality along the RNFL thickness measurements are presented on the TSNIT plots. The probability levels for the RNFL thickness on the TSNIT plot are displayed on a four-color scale with white, green, yellow and red colors displaying progressively thinner RNFL. RNFL measurements at or below the thinnest 1%ile of the measurements from the normative database fall into the red area and are considered to be outside normal limits. RNFL measurements within the thinnest 1–5%ile of the normative database are considered borderline abnormal and are flagged as yellow. Eyes with RNFL measurements within the middle 90%ile of the normative database measurements are considered within normal limits and marked in green. RNFL thickness measurements beyond the 95%ile of the normative database measurements are considered higher than normal and are flagged as white [20].

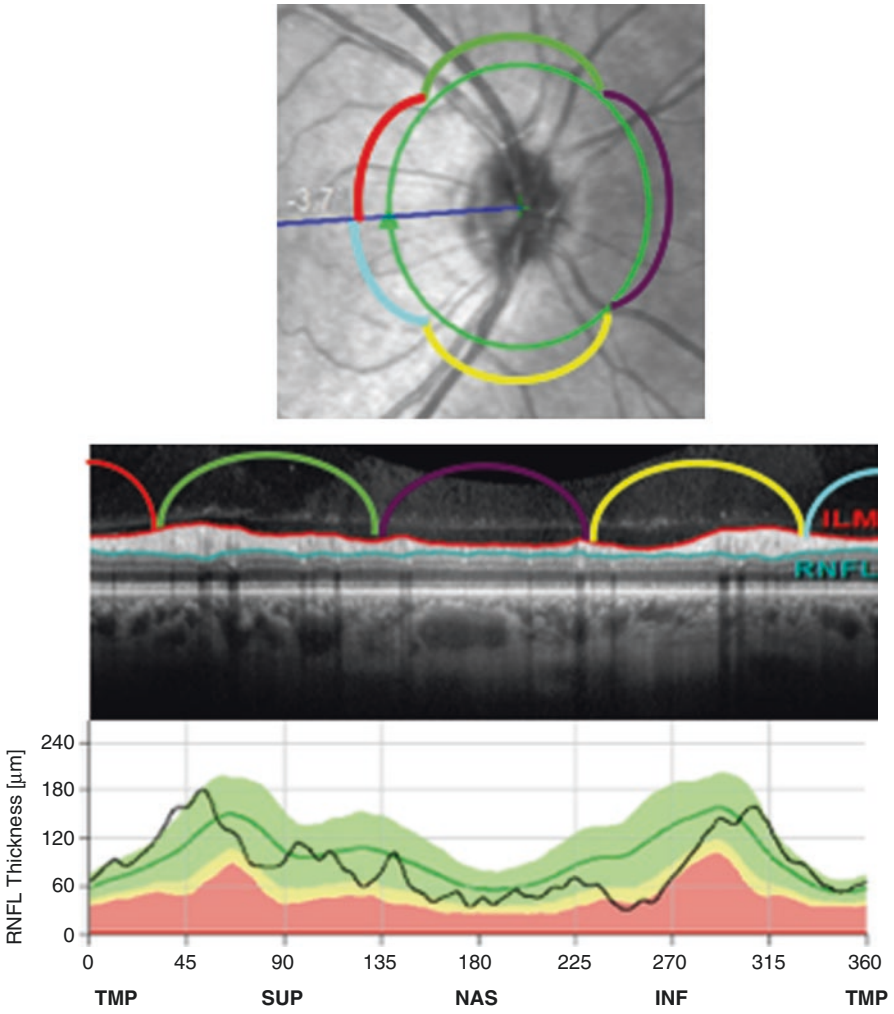

Fig. 3.3 Schematic representation for calculation of a TSNIT map for an RNFL scan from Spectralis OCT

Each manufacturer uses its own normative database values for defining the green, yellow and red areas on the TSNIT maps. Although the layout looks similar, the results cannot be used interchangeably among different devices.

Most of the published papers about the diagnostic capability of OCT in glaucoma use the average and sectorial RNFL thickness data from the calculation circle. In general, the average and inferior quadrant peripapillary RNFL thickness values are the OCT parameters with the best diagnostic accuracy, followed by the superior quadrant RNFL thickness [1, 17, 21, 22]. The test-retest variability of the current SD-OCT systems for the average RNFL thickness is under 5 µm making the average RNFL thickness parameter the most reproducible OCT parameter [23–27]. Using

the quadrant and sector RNFL thickness data for glaucoma diagnosis may increase the sensitivity but decreases the specificity. Average RNFL thickness abnormalities can detect glaucoma with 95% specificity in up to 35% of glaucoma suspect eyes 4 years prior to detectable VF loss and in up to 19% of the eyes, 8 years prior to detectable VF loss [12].

RNFL thickness slowly decreases with age. Normative databases of the commercial OCT systems include RNFL thickness data from different age groups and the RNFL thickness results of each patient is compared with age-matched normative values. In addition to age, axial length and race can influence the distribution of normal RNFL thickness measurements. To overcome this problem, some of the OCT devices include normative data from individuals from different races and varying levels of myopia.

3.3 Macular Ganglion Cell Analysis

More than 50% of the eye's RGCs are located at the macula [28]. The GCL, which is composed of 6 to 8 layers of RGCs constitutes up to 30% to 35% of the total retinal thickness in the macula [27]. RGC loss can be detected in the macula at early stages of glaucoma [28–30]. Importance of the macular region in glaucoma is underestimated as the most frequently used VF testing algorithms such as 30–2 or 24–2 may miss evidence of early glaucomatous damage in the macula and the 10–2 strategy is not commonly used in early disease [31–33]. The reason for the underestimation of early macular damage in glaucoma before SD-OCT became available was the lack of clinical examination methods or imaging techniques that could detect macular damage in glaucoma. TD-OCT's focus was on RNFL thickness measurements, as segmentation of the inner retinal layers was not reliable with the relatively low resolution and the poor sampling density of TD-OCT devices [34]. SD-OCTs overcame the technical difficulties in segmenting macular layers, and macular imaging protocols became an essential part of the diagnostic tools for glaucoma detection. Macular imaging has significant advantages over peripapillary RNFL and ONH parameters in diagnosing glaucoma as it has very low variability and is less prone to artifacts and anatomical variations.

Low reflectivity of the ganglion cell layer is the main challenge for the SD-OCT segmentation algorithms. Since it is difficult to differentiate the GCL and inner plexiform layer (IPL) boundary, and the GCL from RNFL internally, various manufacturers have used different inner retinal layer combinations for diagnosis of glaucoma. Optovue's RT-Vue OCT introduced Ganglion Cell Complex (GCC) thickness measurements. The GCC includes the three innermost layers of the retina; the RNFL, ganglion cell layer and IPL, hence, the GCC contains the axons, cell bodies and dendrites of the ganglion cells that are preferentially affected by glaucoma. Therefore, measuring GCC thickness would be expected to be more sensitive and specific to the disease [35]. Zeiss' Cirrus HD-OCT provides the ganglion cell and inner plexiform layers (GCL + IPL) in its Ganglion Cell Analysis (GCA) software.

This is based on the premise that excluding RNFL from the inner retinal thickness measurements could decrease variability [36].

Heidelberg Engineering Spectralis OCT Posterior Pole Asymmetry analysis was originally able to measure only the total retinal thickness in the macula instead of segmenting different layers of the macula. An intra-eye asymmetry analysis compares the inferior and superior half of the macula [37]. In addition, an inter-eye asymmetry comparison presents one-to-one between-eye differences in superpixel thickness. This method also has a high sensitivity and specificity [38]. The current version of the Spectralis OCT (GMPE) is able to segment individual macular layers separately, but no statistical analysis is provided in the current software.

Topcon Medical Systems manufactures both SD and SS-OCT systems. The SS-OCT system of Topcon, called the DRI-OCT Triton, can scan the peripapillary area and macula in a single 9 × 12mm scan and can measure both GCC and GCL + IPL thickness concurrently.

Introduction of these different segmentation algorithms enhanced the utility and importance of macular OCT imaging. Multiple studies have shown that GCC and GCL + IPL thickness measurements are able to differentiate glaucomatous eyes from normal control eyes with high accuracy [39–42]. Yang et al. showed that both SS-OCT and SD-OCT devices could detect glaucoma with comparable accuracy when compared to peripapillary RNFL measurements [43].

The inferior temporal sector is the most common region displaying GCL + IPL thinning in the macula, which is consistent with the peripapillary area demonstrating RNFL defects most frequently (inferior sectors) [16, 44–46]. As glaucoma deteriorates, arcuate defects and more diffuse damage can be observed in the macula [29, 47].

Although macular ganglion cell OCT compares well to peripapillary RNFL thickness measurements for detection of glaucoma, macular diseases are common in the elderly and disorders such as senile macular degeneration, diabetic maculopathy, and epiretinal membranes may limit the usefulness of macular OCT in glaucoma diagnosis and monitoring. In addition, as the macula contains only 50% of the eye's RGCs, the health of the remaining 50% of RGCs can only be gauges with peripapillary RNFL measurements.

3.4 Optic Nerve Head Analysis

All OCT devices scan the ONH area and provide some information about the ONH health. The scan area and scan properties vary among different OCT devices. Depending on the software algorithm and technical capabilities of the device, different ONH parameters including the cup-to-disc ratio, neuroretinal rim area, and neuroretinal rim volume are provided.

For the ONH analysis, the OCT machine needs to first identify the ONH border. Most current OCT devices consider the BMO as a proxy for the ONH boundary. One reason is the relative ease of identifying the Bruch's membrane on OCT scans.

The segmentation algorithm can fairly easily find the BMO for all available B scans. Identification of the BMO enables the software to determine the centroid of the ONH, which is subsequently used for proper centration of the calculation ring used for RNFL analysis. This method is used by all manufacturers and has a very high repeatability and reproducibility [48, 49]. In addition, identification of the BMO allows the devices to define the optic disc border. After placement of the optic disc border ring, the cup boundary was determined by internal limiting membrane (ILM) termination in some of the earlier OCT devices.

A new definition of the neuroretinal rim area measures the minimum distance from the BMO to ILM and the resulting parameter is called the BMO-MRW (Fig. 3.4) [50, 51].

Zeiss' Cirrus HD-OCT extracts the ONH data from the 200 × 200 Optic Disc Cube scan and has used a concept similar to BMO-MRW since Cirrus HD-OCT optic nerve software was released in 2010. Although this method is widely named as MRW measurement, Cirrus' software minimizes areas instead of distance to determine the neuro-retinal rim border. Cirrus' ONH normative significance limits are corrected for optic disc size and disc tilt. The results are reported in TSNIT type graphs and a summary table for key parameters. On the other hand, Spectralis' original report did not present any information about ONH parameters. ONH analysis became available with the introduction of the GMPE software, which uses the BMO-MRW concept for determining the neuroretinal rim boundaries (Fig. 3.4). The GMPE software can provide geometrically accurate measurements based on 24 radial measurements centered on the BMO centroid (48 data points); this is in contrast to older systems such scanning laser ophthalmoscopy that measured the neuroretinal rim area along or parallel to the fixed plane of the clinical disc margin. The BMO-MRW based approach has a higher diagnostic accuracy for glaucoma and demonstrates a stronger structure-function relationship [51, 52].

The superiority of ONH parameters to RNFL outcomes for diagnosis of early glaucoma is still controversial. While some studies showed ONH parameters to per-

Fig. 3.4 Identification of Bruch's Membrane Opening (BMO) and the BMO-Minimum Rim Width (BMO-MRW) by the GMPE module of Spectralis OCT. The green arrows represent the minimum distance between the termination of the Bruch's membrane and ILM

form better for diagnosing early glaucoma, others found RNFL and macular parameters to perform better [53–55]. ONH parameters are very useful for differential diagnosis of non-glaucomatous optic neuropathies. If an OCT print-out shows RNFL and GCC or GCL + IPL damage while the ONH parameters such as cup-to-disc ratio are within normal limits, non-glaucomatous optic neuropathies must be considered in the differential diagnosis. Chap. 9 will discuss the OCT findings in these glaucoma masqueraders in detail.

Apart from diagnosing glaucoma, SD-OCT technology has greatly improved our understanding of the ONH anatomy. Chauhan and Burgoyne proposed that SD-OCT data represented a paradigm shift for clinical assessment of the ONH [56]. The authors emphasized that a SD-OCT based approach to neuroretinal rim evaluation utilizing the BMO-MRW concept and taking into account the fovea-to-BMO axis angle is anatomically and geometrically more accurate and may enhance glaucoma detection.

Using a combination of RNFL, ONH and macular measurement modalities together can increase the chances of identifying glaucomatous damage early during the disease process. Any one of these parameters can be affected earlier than the others and therefore, taking into account the findings from the RNFL, ONH and macula can enhance early diagnosis of glaucoma [1].

References

1. Dong ZM, Wollstein G, Schuman JS. Clinical utility of optical coherence tomography in Glaucoma. Invest Ophthalmol Vis Sci. 2016:57–67.
2. Quigley HA, Addicks EM, Green WR. Optic nerve damage in human glaucoma III. Quantitative correlation of nerve fiber loss and visual field defect in glaucoma, ischemic neuropathy, papill-edema, and toxic neuropathy. Arch Ophthalmol. 1982;100:135–46.
3. Hood DC, Kardon RH. A framework for comparing structural and functional measures of glaucomatous damage. Prog Retina Eye Res. 2007;26:688–710.
4. Sommer A, Katz J, Quigley HA, Miller NR, Robin AL, Richter RC, Witt KA. Clinically detectable nerve fiber atrophy precedes the onset of glaucomatous field loss. Arch Ophthalmol. 1991;109:77–83.
5. Kamal DS, Viswanathan AC, Garway-Heath DF, Hitchings RA, Poinoosawmy D, Bunce C. Detection of optic disc change with the Heidelberg retina tomograph before confirmed visual field change in ocular hypertensives converting to early glaucoma. Br J Ophthalmol. 1999;83:290–4.
6. Philippin H, Unsoeld A, Maier P, Walter S, Bach M, Funk J. Ten-year results: detection of long-term progressive optic disc changes with confocal laser tomography. Graefes Arch Clin Exp Ophthalmol. 2006;244:460–4.
7. Sehi M, Greenfield DS. Assessment of retinal nerve fiber layer using optical coherence tomography and scanning laser polarimetry in progressive glaucomatous optic neuropathy. Am J Ophthalmol. 2006;142:1056–9.
8. Wollstein G, Schuman JS, Price LL, Aydin A, Stark PC, Hertzmark E, Lai E, Ishikawa H, Mattox C, Fujimoto JG, Paunescu LA. Optical coherence tomography longitudinal evaluation of retinal nerve fiber layer thickness in glaucoma. Arch Ophthalmol. 2005;23:464–70.

9. Strouthidis NG, Scott A, Peter NM, Garway-Heath DF. Optic disc and visual field progression in ocular hypertensive subjects: detection rates, specificity, and agreement. Invest Ophthalmol Vis Sci. 2006;47:2904–10.
10. Quigley HA, Katz J, Derick RJ, Gilbert D, Sommer A. An evaluation of optic disc and nerve fiber layer examinations in monitoring progression of early glaucoma damage. Ophthalmology. 1992;99:19–28.
11. Medeiros FA, Alencar LM, Zangwill LM, Bowd C, Sample PA, Weinreb RN. Prediction of functional loss in glaucoma from progressive optic disc damage. Arch Ophthalmol. 2009;127:1250–6.
12. Kuang TM, Zhang C, Zangwill LM, Weinreb RN, Medeiros FA. Estimating lead ime gained by optical coherence tomography in detecting Glaucoma before development of visual field defects. Ophthalmology. 2015;122:2002–9.
13. Weinreb RN, Garway-Heath DF, Leung C, Mederios FA, Liebmann J. Diagnosis of primary open angle glaucoma, World Glaucoma association Consesus Series, vol. 10. Amsterdam, The Netherlands: Kugler Publications; 2016.
14. Fortune B, Burgoyne CF, Cull GA, Reynaud J, Wang L. Structural and functional abnormalities of retinal ganglion cells measured in vivo at the onset of optic nerve head surface change in experimental glaucoma. Invest Ophthalmol Vis Sci. 2012;53:3939–50.
15. Huang D, Swanson EA, Lin CP, Schuman JS, Stinson WG, Chang W, Hee MR, Flotte T, Gregory K, Puliafito CA, Fujimoto JG. Optical coherence tomography. Science. 1991;254(5035):1178–81.
16. Leung CK. Diagnosing glaucoma progression with optical coherence tomography. Curr Opin Ophthalmol. 2014;25:104–11.
17. Leung CK, Yu M, Weinreb RN, Lai G, Xu G, Lam DS. Retinal nerve fiber layer imaging with spectral-domain optical coherence tomography: patterns of retinal nerve fiber layer progression. Ophthalmology. 2012;119:1858–66.
18. Leung CK, Lam S, Weinreb RN, Liu S, Ye C, Liu L, He J, Lai GW, Li T, Lam DS. Retinal nerve fiber layer imaging with spectral-domain optical coherence tomography: analysis of the retinal nerve fiber layer map for glaucoma detection. Ophthalmology. 2010;117:1684–91.
19. Schuman JS, Pedut-Kloizman T, Hertzmark E, Hee MR, Wilkins JR, Coker JG, Puliafito CA, Fujimoto JG, Swanson EA. Reproducibility of nerve fiber layer thickness measurements using optical coherence tomography. Ophthalmology. 1996;103:1889–98.
20. Zeiss Cirrus HD-OCT User Manual – Models 500, 5000 Instrument and Review Software 8.1, 2015, p. 179.
21. Wang X, Li S, Fu J, Wu G, Mu D, Li S, Wang J, Wang N. Comparative study of retinal nerve fiber layer measurement by RTVue OCT and. GDx VCC Br J Ophthalmol. 2011;95:509–5.
22. Rao HL, Zangwill LM, Weinreb RN, Sample PA, Alencar LM, Medeiros FA. Comparison of different spectral domain optical coherence tomography scanning areas for glaucoma diagnosis. Ophthalmology. 2010;117:1692–9.
23. Leung CK, Cheung CY, Weinreb RN, Qiu Q, Liu S, Li H, Xu G, Fan N, Huang L, Pang CP, Lam DS. Retinal nerve fiber layer imaging with spectral-domain optical coherence tomography: a variability and diagnostic performance study. Ophthalmology. 2009;116:1257–63.
24. Mwanza J, Chang R, Budenz D, et al. Reproducibility of peripapillary retinal nerve fiber layer thickness and optic nerve head parameters measured with Cirrus HD-OCT in glaucomatous eyes. Invest Ophthalmol Vis Sci. 2010;51:5724–30.
25. Horne MR, Callan T, Durbin M, Abunto T. Inter-visit and Inter-instrument variability for CIRRUS HD-OCT Peripapillary retinal nerve Fiber layer thickness measurements. ARVO 2008 Abstracts, Invest Ophthalmol Vis Sci. 2008;49:4624.
26. Tan BB, Natividad M, Chua KC, Yip LW. Comparison of retinal nerve fiber layer measurement between 2 spectral domain OCT instruments. J Glaucoma. 2012;21:266–73.
27. Wu H, de Boer JF, Chen TC. Reproducibility of retinal nerve Fiber layer thickness measurements using spectral domain optical coherence tomography. J Glaucoma. 2011;20:470–6.

28. Curcio CA, Allen KA. Topography of ganglion cells in human retina. J Comp Neurol. 1990;300:5–25.
29. Hood DC, Slobodnick A, Raza AS, de Moraes CG, Teng CC, Ritch R. Early glaucoma involves both deep local, and shallow widespread, retinal nerve fiber damage of the macular region. Invest Ophthalmol Vis Sci. 2014;55:632–6.
30. Hood DC, Raza AS, de Moraes CG, Liebmann JM, Ritch R. Glaucomatous damage of the macula. Prog Retin Eye Res. 2013;32:1–21.
31. Traynis I, De Moraes CG, Raza AS, Liebmann JM, Ritch R, Hood DC. Prevalence and nature of early glaucomatous defects in the central 10 degrees of the visual field. JAMA Ophthalmol. 2014;132:291–29.
32. Grillo LM, Wang DL, Ramachandran R, Ehrlich AC, De Moraes CG, Ritch R, Hood DC. The 24-2 visual field test misses central macular damage confirmed by the 10-2 visual field test and optical coherence tomography. Translational Vision Science & Technology. 2016;5:15.
33. De Moraes CG, Hood DC, Thenappan A, Girkin CA, Medeiros FA, Weinreb RN, Zangwill LM, Liebmann JM. 24-2 visual fields miss central defects shown on 10-2 tests in glaucoma suspects, ocular hypertensives, and early glaucoma. Ophthalmology. 2017;124:1449–56.
34. Medeiros FA, Zangwill LM, Bowd C, Vessani RM, Susanna R Jr, Weinreb RN. Evaluation of retinal nerve fiber layer optic nerve head, and macular thickness measurements for glaucoma detection using optical coherence tomography. Am J Ophthalmol. 2005;139:44–55.
35. Tan O, Chopra V, Lu AT, Schuman JS, Ishikawa H, Wollstein G, Varma R, Huang D. Detection of macular ganglion cell loss in glaucoma by Fourier-domain optical coherence tomography. Ophthalmology. 2009;116:2305–14.
36. Mwanza JC, Oakley JD, Budenz DL, Chang RT, Knight OJ, Feuer WJ. Macular ganglion cell–inner plexiform layer: automated detection and thickness reproducibility with spectral domain–optical coherence tomography in Glaucoma. Invest Ophthalmol Vis Sci. 2011;52:8323–9.
37. Asrani S, Rosdahl JA, Allingham RR. Novel software strategy for glaucoma diagnosis: asymmetry analysis of retinal thickness. Arch Ophthalmol. 2011;129:1205–11.
38. Seo JH, Kim TW, Weinreb RN, Park KH, Kim SH, Kim DM. Detection of localized retinal nerve fiber layer defects with posterior pole asymmetry analysis of spectral domain optical coherence tomography. Invest Ophthalmol Vis Sci. 2012;53:4347–53.
39. Mwanza JC, Durbin MK, Budenz DL, Sayyad FE, Chang RT, Neelakantan A, Godfrey DG, Carter R, Crandall AS. Glaucoma diagnostic accuracy of ganglion cell-inner plexiform layer thickness: comparison with nerve fiber layer and optic nerve head. Ophthalmology. 2012;119:1151–8.
40. Schulze A, Lamparter J, Pfeiffer N, Berisha F, Schmidtmann I, Hoffmann EM. Diagnostic ability of retinal ganglion cell complex, retinal nerve fiber layer, and optic nerve head measurements by Fourier-domain optical coherence tomography. Graefes Arch Clin Exp Ophthalmol. 2011;249:1039–10.
41. Sung KR, Wollstein G, Kim NR, Na JH, Nevins JE, Kim CY, Schuman JS. Macular assessment using optical coherence tomography for glaucoma diagnosis. Br J Ophthalmol. 2012;96:1452–5.
42. Garas A, Vargha P, Hollo G. Diagnostic accuracy of nerve fiber layer macular thickness and optic disc measurements made with the RTVue-100 optical coherence tomograph to detect glaucoma. Eye (Lond). 2011;25:57–65.
43. Yang Z, Tatham AJ, Weinreb RN, Medeiros FA, Liu T, Zangwill LM. Diagnostic ability of macular ganglion cell inner plexiform layer measurements in glaucoma using swept source and spectral domain optical coherence tomography. PLoS One. 2015;10:e0125957.
44. Tan O, Li G, Lu AT, Varma R, Huang D. Advanced imaging for Glaucoma study group. Mapping of macular substructures with optical coherence tomography for glaucoma diagnosis. Ophthalmology. 2008;115:949–56.
45. Hood DC, Raza AS, de Moraes CG, Johnson CA, Liebmann JM, Ritch R. The nature of macular damage in glaucoma as revealed by averaging optical coherence tomography data. Translational Vision Science & Technology. 2012;1:3.

46. Kotera Y, Hangai M, Hirose F, Mori S, Yoshimura N. Three-dimensional imaging of macular inner structures in glaucoma by using spectral-domain optical coherence tomography. Invest Ophthalmol Vis Sci. 2011;52:1412–4.
47. Wang DL, Raza AS, de Moraes CG, Chen M, Alhadeff P, Jarukatsetphorn R, Ritch R, Hood DC. Central glaucomatous damage of the macula can be overlooked by conventional OCT retinal nerve fiber layer thickness analyses. Translational Vision Science & Technology. 2015;4:4.
48. Reis AS, Sharpe GP, Yang H, Nicolela MT, Burgoyne CF, Chauhan BC. Optic disc margin anatomy in patients with glaucoma and normal controls with spectral domain optical coherence tomography. Ophthalmology. 2012;119:738–47.
49. Almobarak FA, O'Leary N, Reis AS, Sharpe GP, Hutchison DM, Nicolela MT, Chauhan BC. Automated segmentation of optic nerve head structures with optical coherence tomography. Invest Ophthalmol Vis Sci. 2014;55:1161–8.
50. Chauhan BC, Danthurebandara VM, Sharpe GP, Demirel S, Girkin CA, Mardin CY, Scheuerle AF, Burgoyne CF. Bruch's's membrane opening-minimum rim width and retinal nerve fibre layer thickness in a normal white population. A multi-Centre study. Ophthalmology. 2015;122:1786–94.
51. Chauhan BC, O'Leary N, Almobarak FA, Reis AS, Yang H, Sharpe GP, Hutchison DM, Nicolela MT, Burgoyne CF. Enhanced detection of open-angle glaucoma with an anatomically accurate optical coherence tomography-derived neuroretinal rim parameter. Ophthalmology. 2013;120:535–43.
52. Pollet-Villard F, Chiquet C, Romanet JP, Noel C, Aptel F. Structure-function relationships with spectral-domain optical coherence tomography retinal nerve fiber layer and optic nerve head measurements. Invest Ophthalmol Vis Sci. 2014;55:2953–62.
53. Kasumovic SS, Pavljasevic S, Cabric E, Mavija M, Dacic-Lepara S, Jankov M. Correlation between retinal nerve fiber layer and disc parameters in glaucoma suspected eyes. Med Arch. 2014;68:113–1.
54. Sung KR, Na JH, Lee Y. Glaucoma diagnostic capabilities of optic nerve head parameters as determined by Cirrus HD optical coherence tomography. J Glaucoma. 2012;21:498–504.
55. Lisboa R, Paranhos A Jr, Weinreb RN, Zangwill LM, Leite MT, Medeiros FA. Comparison of different spectral domain OCT scanning protocols for diagnosing preperimetric glaucoma. Invest Ophthalmol Vis Sci. 2013;54:3417–34.
56. Chauhan BC, Burgoyne CF. From clinical examination of the optic disc to clinical assessment of the optic nerve head: a paradigm change. Am J Ophthalmol. 2013;156:218–27.